RING-FAULT DELINEATION OF AN ANCIENT VOLCANIC CALDERA BASED ON 3-D GRAVITY INVERSE MODELING IN MAJENANG REGION, INDONESIA

Accep Handyarso[1, 2, *]
[1]*Geological Resources Research Center, National Research and Innovation Agency of the Republic of Indonesia. Jalan Sangkuriang, Bandung, Indonesia. 40135*
[2]*Ex-Center for Geological Survey, Geological Agency, Ministry of Energy and Mineral Resources (MEMR) of the Republic of Indonesia. Jalan Diponegoro, Bandung, Indonesia. 40122*
**Email corresponding: accep.handyarso@brin.go.id*

How to cite: A. Handyarso, "Ring-fault delineation of an ancient volcanic caldera based on 3-D gravity inverse modeling in the Majenang region, Indonesia" *Kurvatek*, vol. 7, no. 2, pp. 103 - 114, 2022. doi: 10.33579/krvtk.v7i2.3197 [Online].

Abstract — Calderas are important geological features in all volcanic environments due to give directives clues of geological resources such as geothermal system, mineralization, or even in oil and gas potential reserved. The ability of recognizing these specific features play an important role in the exploration activities. A good understanding of the geological settings will bring to the right direction and make the exploration activities becomes optimized and cost effective. Gravity method is commonly used for preliminary study almost of any cases due to lightweight, low-cost, and the ability to figure out a wide region quickly. Gravity method has an excellent lateral resolution but it has limitation with the vertical resolution. Applying depth-weighting mechanism makes, the inverse-modeling result becomes interpretable. According to the research, there is a northwest-southeast dextral strike-slip fault in the area, which belongs to the Pamanukan-Cilacap Fault Zone (PCFZ). A Circular anomaly pattern also delineated and interpreted as the ring-fault of an ancient volcanic caldera in the study area. Several high gravity anomaly located within the caldera-rims are interpreted as the lava domes or intrusion rocks. The eruption center point estimated at around the Majenang city. The PCFZ behaves as the weak zones in the area where the magmatism rise through and create the ancient volcano, which now remain as the Majenang Caldera.

Keywords: Gravity, Caldera, Ring-Fault, Geological-Resources, Indonesia.

I. INTRODUCTION

The Gravity method is one of the geophysical methods, which is widely used for a preliminary study of an area in many specific purposes such as oil and gas exploration, mineral exploration, geothermal exploration, fault delineation, volcanology applications, etc. Such widespread of usage led to the emergence of gravity inversion schemes diversity. Generally, various gravity inversion purposes divided into sediment thickness (or basement depth) estimation and density contrast distribution estimation below the surface. A compact gravity inversion, which numerically stable and convergent rapidly is successful to generate a more focused causative body source as the inversion result and compared to the drill log dataset [1]. A growing body gravity inversion built with pre-assignment density contrast into the algorithm. The proposed method was examined by the synthetics dataset and field dataset in the Volcanic Island of Gran Canaria (Canary Island, Spain) with a satisfactory result [2]. A similar growing body inversion method called the planting anomalies density proposed in 2012. The method invokes gradient computation as the additional way to estimate a 3D density-contrast distribution below the surface [3]. The planting density anomaly successfully applied to the iron ore estimation in Brazil. All mentioned inversion schemes are categorized as the inversion for density contrast distribution estimation. The earliest example of the cross-sectional shape of the sedimentary basin [4] can be categorized as the surface inversion of gravity dataset, which then improved into 3D surface inversion [5]. The method was applied to the entire state of Nevada in order to analyze the shape and distribution of basins [6]. The similar method was also implemented to estimate the thickness of concealed sedimentary deposits beneath the Columbia River Basalt Group in Washington State [7]. Further, the Bott method was modified as the Maximum Difference Reduction (MDR) with an additional function called absolute maximum regularization of the misfit data [8]. The Bott method uses the Bouguer slab as a major determinant of depth perturbation, while the MDR method uses the misfit value

Received July 20, 2022; Revised September 9, 2022; Accepted November 7, 2022

that is normalized by absolute maximum regularization at each iteration. The MDR method developed further to consider any regularization such as smoothness and or total variation into calculation including the uses of Trend Surface Analysis (TSA) to invert gravity dataset directly from the Bouguer anomaly [9]. The calculation scheme invoke the Gauss-Newton inversion approach transformation, where the Bott method successfully transformed and regularized [10]. Any other regularization type such as minimum support, gradient minimum support, minimum entropy, etc are possible to be applied [11, 12]. The gravity inverse modeling proved has been applied as the solution of various earth problems and has undergone many significant developments.

A subsurface modeling based on the gravity dataset was conducted in the Majenang region, Central Java, Indonesia. Majenang region becomes part of the Banyumas Basin that is believed as one of the prospect sedimentary basins in Indonesia. Nevertheless, the area is covered by thick volcanic sediment. It was reported that the volcanic activities in Java Island have been started since the Cretaceous Period up to the Neogene or even Quaternary Period [13]. The same result was also reported that the volcanism has been started since the late Eocene to early Miocene in the Java Island without explaining about its intensity [14]. According to the volcanic fragment counting of several rock formations around North Serayu Basin, i.e., Worawari Formation as the Eocene–Oligocene epoch, Merayu Formation as the Miocene epoch, and Penyatan Formation as the Pliocene epoch shows that the volcanic activity increase from the older rock formations to the younger rock formations [15].

Exploration of any prospective area needs an understanding of the geological-setting around the targeted zone. Almost all of the prospected area is covered by thick volcanic sediment, including the study area in the Majenang region, Central Java, Indonesia. The thick volcanic sediment imply that there must be hidden or unidentified place around the area which produces the volcanic sediment. In other words, there must be an ancient volcano and its eruption point as the source of the existing volcanic rocks or sediments in the area. These geological features should be identified before doing exploration activities. This step is quite important to reduce the exploration risk, especially related to the area, which is covered by thick volcanic sediments. The purpose of this paper is to study and identify the Majenang region, Central Java, Indonesia as one of the former ancient volcanoes based on gravity methods. A further study is needed to describe the geological-setting in the Majenang region. Especially in defining the ancient volcanic caldera boundary and its eruption center point, which generate the thick volcanic sediments in the area.

II. METHODS

A. Forward Modeling

Gravity forward modeling is a linear problem that can be calculated by performing integration of the gravity field vertical component according to the given density block. The gravity meter measures the vertical attraction of the gravity ($g(x,y,z)$) in other words, the gravity anomaly is a vertical gradient of the gravity potential (U) in a datum measurement point as shown in Eq. 1–5. The equation shows that the gravity anomaly is a superposition of all density elements beneath the surface marked with a triple integral due to in Cartesian coordinate [16].

$$g(x,y,z) = \frac{\partial U}{\partial z} \tag{1}$$

$$g(x,y,z) = -\gamma \iiint \rho(x',y',z') \frac{(z-z')}{r^3} dx'dy'dz' \tag{2}$$

where

$$r = \sqrt{(x-x')^2 + (y-y')^2 + (z-z')^2} \tag{3}$$

A simplification to the geometry within the equation generate a kernel function, which also knows as the Green function. The Eq. 4 becomes the general form of the gravity anomaly formula for forward modeling calculations. The Eq. 4 expressing the gravitational anomaly due to a point mass located at (x',y',z') with a given density contrast $\rho(x',y',z')$. The Eq. 5 is the part called as the Green function or a kernel function for the calculation.

$$g(x,y,z) = \iiint \rho(x',y',z')\psi(x-x',y-y',z-z')\, dx'dy'dz' \tag{4}$$

where

$$\psi(x,y,z) = -\gamma \frac{z}{(x^2+y^2+z^2)^{3/2}} \tag{5}$$

Further implementation of the Eq. 4 within the computational range can be expressed as the summation of multiplication operation as shown in Eq. 6.

$$g_m = \sum_{n=1}^{N} \rho_n \psi_{mn} \quad (6)$$

where g_m is the vertical attraction of gravity field at the m^{th} observation point, ρ_n is the density contrast of the n^{th} cell discretization, and ψ_{mn} is the gravitational attraction at point m^{th} due to n^{th} cell with unity density contrast value.

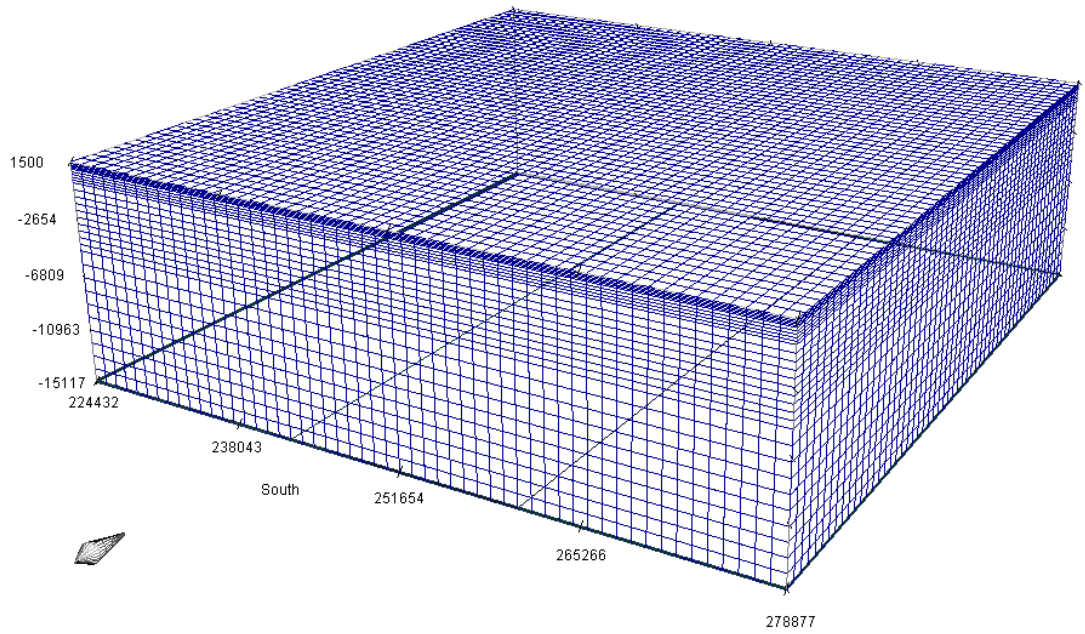

Figure 1. Discretization the subsurface into a number of prisms called as pixel cell which keep density value.

B. Inverse Modeling

The gravity inverse modeling can be classified into the linear inverse problem or non-linear inverse problem. The density contrast estimation beneath an area in any form can be categorized as the linear inverse problem, while the surface inversion or basement depth estimations are categorized as the non-linear inverse problem. A non-linear inverse problem can be solved with linearization approach as well as a linear inverse problem known as Newton method, Gauss-Newton method, Gradient Method (steepest ascent & steepest descent), Levenberg-Marquardt method, and any other variants [17].

Density contrast distribution estimation beneath the surface can be expressed in a linear form where the model response (d) acquired as a simply multiplication between the Green function (G) and the model parameter (m). According to the Eq. 6, there is a linear relations between the vertical attraction of the gravity field (g_m) with the density contrast distribution (ρ_n) and the geometry which represented by the Green function (ψ_{mn}). Redefining new variables $d = [d_1, d_2, d_3, d_4, \dots d_N]$ as the vertical gravity attraction dataset (g_m), $m = [\rho_1, \rho_2, \rho_3, \rho_4, \dots \rho_M]$ as the density contrast for each discretized cell beneath the surface or simple called as the model parameter (ρ_n) as shown in Figure 1, and the Green function (ψ_{mn}) defined as G parameter. Hence the data and model parameter relationship in the Eq. 6 can be rewrite as the Eq. 7.

$$d = Gm \quad (7)$$

The G parameter in Eq. 7 do a model parameter m mapping into the correspond data point d or in other words, we can predict the model parameter m using the G parameter according to the given dataset d. The inversion scheme should minimized the error or the difference between observed data d^{obs} and calculated data d^{calc}. In the sense of Least Square minimization, the error function expressed in Eq. 8 and the solution of the equation is the stationary value to the model parameter, which is expressed in the Eq. 9.

$$E = e^T e = [d^{obs} - d^{calc}]^T [d^{obs} - d^{calc}] = [d^{obs} - Gm]^T [d^{obs} - Gm] \quad (8)$$

$$m = [G^T G]^{-1} G^T d \quad (9)$$

Eq. 9 is the solution for linear inversion in the inverse problem given in Eq. 7. Stability problem may came out when the $[G^T G]$ is a singular matrix, which needs special handling with certain method such as Gauss-Jordan elimination, LU decomposition, Singular Value Decomposition (SVD) etc. Practically, avoiding instability problem during the inverse problem computation can be done by add a small value into the $[G^T G]$ in such way it can prevent too small Eigen value, which causing a large amount number or an infinity when inversed. Hence, the Eq. 9 can be rewrite as the Eq. 10 with a ε^2 value to increase its stability during calculation. The new equation known as the damped linear inversion.

$$m = [G^T G + \varepsilon^2 I]^{-1} G^T d \tag{10}$$

C. Regularization

A damping factor ε^2 in Eq. 10 widely known as the regularization parameter within an inversion. Determination of the damping factor ε^2 can be done under trial and error or using an optimization ways, L-Curve method. The L-Curve method is plotted the inversion results into an error as the horizontal axis and model norm as the vertical axis. The damping factor ε^2 selected should minimalized both the data error and model norm. Commonly, the optimum value to minimalize both error misfit and model norm located at the knee point of the L-Curve. This point also known as the trade-off value on the L-Curve. Further implementation of the regularization performed by modification the identity matrix I in the Eq. 10. There are several regularization method, which is commonly used as the smoothness, total variation, minimum support, gradient minimum support, etc [11].

$$L_1 = \begin{bmatrix} -1 & 1 & 0 & \cdots & 0 \\ 0 & -1 & 1 & & \\ \vdots & & \ddots & & \vdots \\ & & -1 & 1 & 0 \\ 0 & \cdots & 0 & -1 & 1 \end{bmatrix} \tag{11}$$

$$L_2 = \begin{bmatrix} 1 & -2 & 1 & 0 & \cdots & & 0 \\ 0 & 1 & -2 & 1 & & & \\ \vdots & & & & & & \\ & & & \ddots & & & \\ & & & & & & \vdots \\ & & & 1 & -2 & 1 & 0 \\ 0 & & \cdots & 0 & 1 & -2 & 1 \end{bmatrix} \tag{12}$$

$$L_3 = \begin{bmatrix} -1 & 3 & -3 & 1 & 0 & \cdots & 0 \\ 0 & -1 & 3 & -3 & 1 & & \\ \vdots & & & & & & \\ & & & \ddots & & & \\ & & & & & & \vdots \\ & & -1 & 3 & -3 & 1 & 0 \\ 0 & & \cdots & -1 & 3 & -3 & 1 \end{bmatrix} \tag{13}$$

The regularization concepts based on the model norm makes it possible to apply initial model as the model reference in the calculation. In this way, geological constraints can be included as a prior information. In certain cases, the spatial variation of the solution model parameters expected has narrow variation, such that the difference of the solution model parameter that is located in adjacent should be minimized. In this case, “compact” or “smooth” ones generated depends on the differential operator applied to calculate the difference of the variation. There are several differential operator choices which commonly used within the inversion, i.e. the L_1, L_2, and L_3 as shown in Eq. 11 – Eq. 13.

The given Eq. 11, Eq. 12, and Eq. 13 are the differential operator, which mostly used within an inverse modeling calculation. The L_1 operator known as the Total Variation (TV) regularization or sometimes can be utilized for compactness regularization. In another reference, it is mentioned as the flatness regularization. The L_2 operator is the smoothness regularization operator, while the L_3 as the third order norm but rarely used in the applications. The higher order of the norm model used will affect to the shape of the calculation where the higher norm is less robust to dealing with the outliers in our data. The L_1 norm is most robust or less sensitive where the outliers present in the data [17]. This point should be considered when executing an inverse modeling during the data processing and interpretation.

III. RESULTS AND DISCUSSION

A. Synthetics Dataset

The 3-D Gravity inversion is examined with the synthetically model to know its characteristic, especially related to the depth weighting result and gravity anomaly response due to geological structures. The synthetics model is designed to simulate the strike-slip fault existence beneath an area. Strike-slip faults are thought to be present in the study area. Gaussian noise with 1.0 mGal standard deviations was added into the response model generated to simulate the reading and instrument variations. A uniform weighting is applied to every datum points calculated during the forward calculation.

Table 1. Dimension of the causative body beneath the surface

	Prism #1 (m)		Prism #2 (m)	
X (easting)	241572.080	254679.200	250646.240	263753.360
Y (northing)	9179240.470	9197381.410	9197381.410	9215522.350
Z (depth)	-2519.565	-4535.217	-2519.565	-4535.217
P (density)	0.7 kg/m^3		0.7 kg/m^3	

The blocky density model is consisting of two prisms body sources below the surface with the same density contrast value as shown in Table 1. The density contrast value used for the synthetics data is 0.7 kg/m^3. The dimension of each prismatic body source are equivalent but the location beneath the surface is designed as if a net-slip presence in the model. Overall, the subsurface model has a north-south lineament which is strike-slip faulted in the west-east direction as shown in Figure 2. The depth of the body sources model is around 2.5 Km up to 4.5 Km.

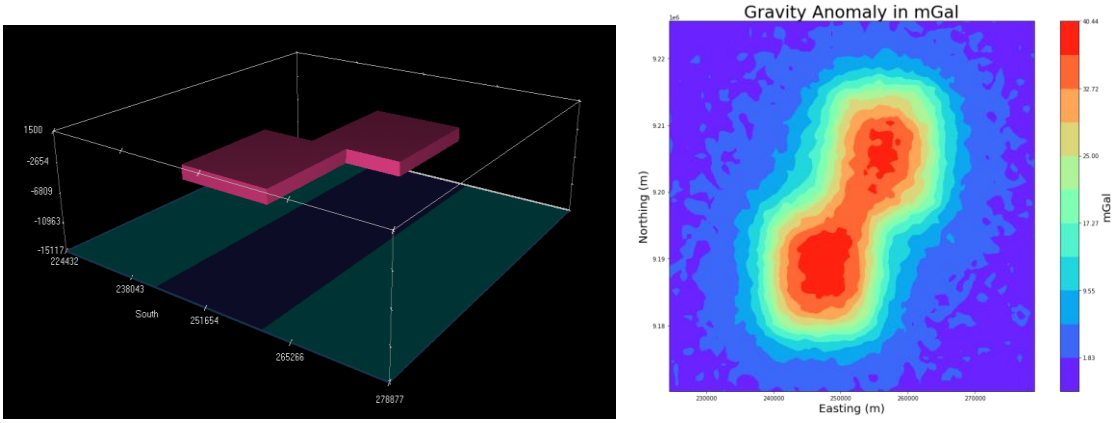

(a) (b)

Figure 2. The gravity synthetic modeling due to strike-slip fault subsurface model, which is represented by two blocky model (a), and gaussian noise 1 mGal is applied to the model response produced (b).

The gravity model response shown in Figure 2 is calculated based on the Eq. 4, which has been defined in the discret form as expressed in Eq. 14. The gravity response of the 3D rectangular prism at a point $P(0,0,0)$ at the origin of Cartesian coordinate system is calculated by using the equation given as follow [16]:

$$g_z = G\Delta\rho \sum_{k=1}^{2}\sum_{j=1}^{2}\sum_{i=1}^{2}\mu_{ijk}\left[z_k tan^{-1}\frac{x_i y_j}{z_k R_{ijk}} - x_i log\left(R_{ijk}+y_j\right) - y_j \log\left(R_{ijk}+x_i\right)\right] \quad (14)$$

where $G = 6.67x10^{-11}m^3kg^{-1}s^{-2}$ is the universal gravity constant, $\Delta\rho$ is the density contrast assignment value, which is constant for the whole causative body, $\mu_{ijk} = (-1)^i(-1)^j(-1)^k$, (x_i, y_j, z_k) are the east, north and depth (vertical) directions respectively, and $R_{ijk} = \sqrt{{x_i}^2 + {y_j}^2 + {z_k}^2}$.

The inverse modeling of the synthetic dataset is conducted with two kinds of model norm regularization. The smooth and compact model norm regularization is commonly used in many cases. The smoothness regularization gives a density gradation around the mass center of the model while the compactness regularization is relatively focused on the mass point of the causative body. The compactness regularization

is quite similar to the minimum support regularization, which valid for the smallest number of the active cell in the model but consistently gives a matched calculated data to the observed dataset. Comparison is made to the inverse modeling result with smoothness and compactness regularization to the true model as shown in Figure 3. Figure 3 displays the inversion result from the top point of view, while Figure 4 displayed the inversion result for both smoothness and compactness regularization in the 3-D perspectives view.

The compact regularization gives more focused causative bodies rather than the smoothness regularization. These results can be seen from both Figure 3 and Figure 4. According to the Figure 4, the smoothness regularization has bigger model variance near the surface rather than the compactness regularization. In this case, the depth-weighting applied better in compactness regularization.

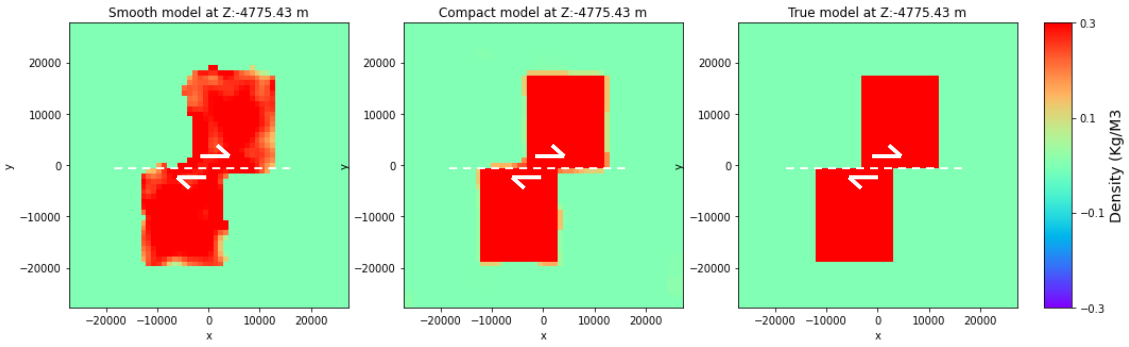

Figure 3. The inverse modeling comparison between smoothness and compactness regularization result as well as the true model for comparison plotted within density contrast of ±0.3 kg/m^3.

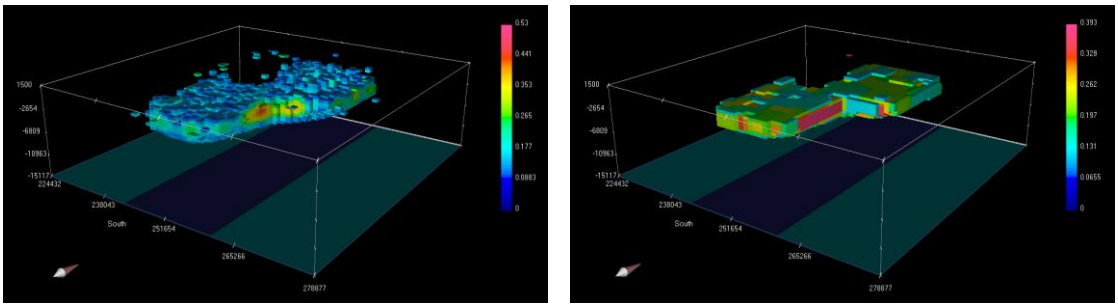

(a) (b)

Figure 4. The inversion result both smoothness (a) and compactness (b) regularization visualized in the 3-D perspective view and close with the true model in Figure 2a.

Qualitatively, the inversion results can resolve the true model in Figure 2a with two kinds of regularization, i.e. smoothness and compactness regularizations as shown in Figure 3 and Figure 4. This indicates that the inversion schemes can be used for field dataset applications. The difference point is the density contrast of the inversion result is smaller than the density contrast assigned to the true model. Nevertheless, the bigger causative body volume as the inversion result compensates the smaller density contrast and give a matched gravity anomaly as the model responses for both the inversion results.

B. Field Dataset

The study area covered the region from 108.5° E to 109.0° E and from 7.0° S to and 7.5° S as shown in the Figure 5. According to the Geological Map Index published by Center for Geological Survey, the study area located at Geological Map of Majenang Quadrangle scale 1:100000 where surrounded by Cirebon Quadrangle at the north, Pangandaran Quadrangle at the south, Tasikmalaya Quadrangle at the west, and Purwokerto Quadrangle at the east. Overally, the study area located at the western part of Central Java, Indonesia. Earth scientists believe that the study area reserved economic potential resources but mostly covered by volcanic sediments.

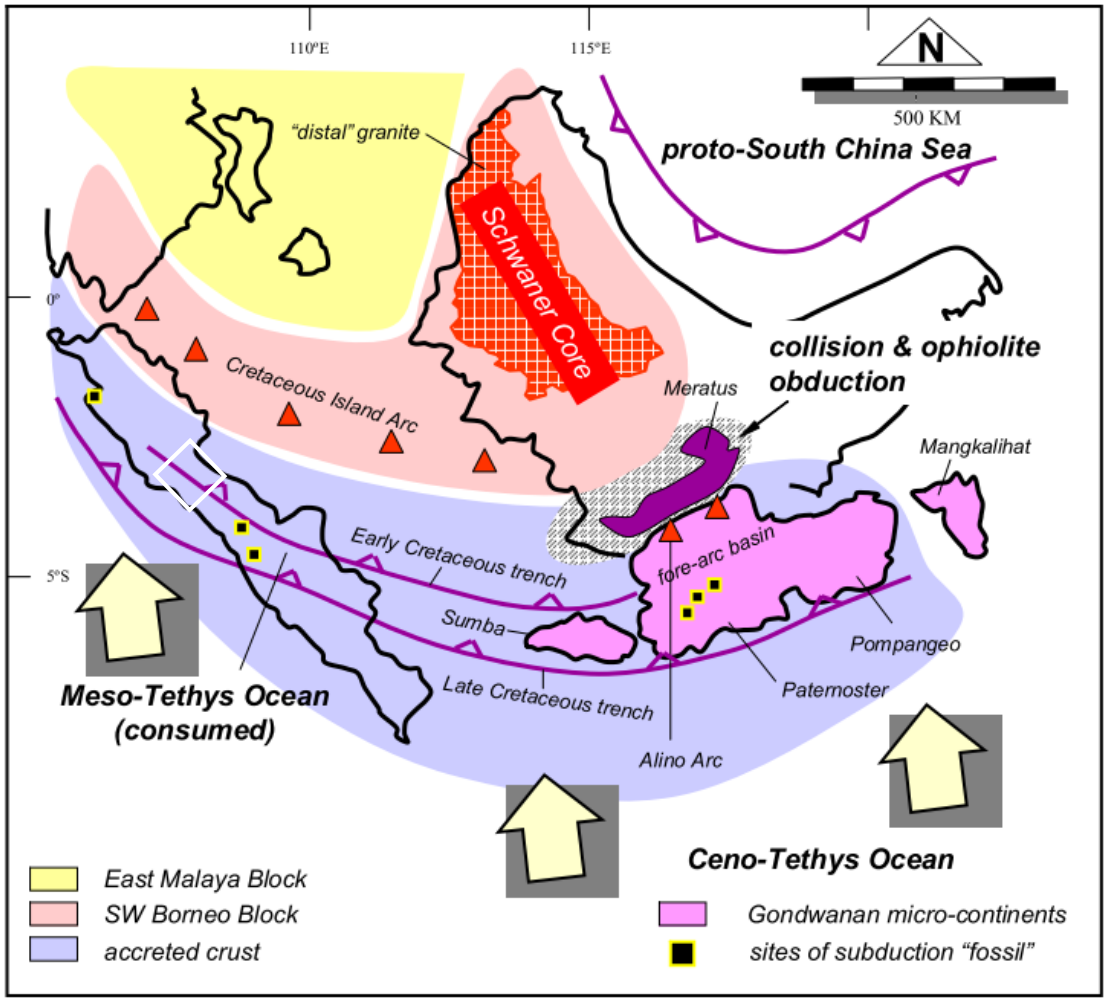

Figure 5. Paleo-tectonic reconstruction of the southeastern part of Sundaland and its accreted crust during Cretaceous [20]. The white box represents the study area presented in this paper.

Java Island was formed in the late Mesozoic-Cenozoic era. The magmatic arc in Java Island has shifted as the impact of subduction zone displacement from the southern to the northern part of the island during the Tertiary-Quaternary period [14, 18, 19, and 20]. In the Cretaceous-early Eocene, the magmatic arc location was in the northern part of West Java, such that the Bogor depression to be the Fore Arc Basin is marked with the red zone as shown in Figure 5. The magmatic arc in the late Eocene-early Miocene was located at the southern part of Java Island, while in the late Miocene-Pliocene the magmatic arc shifted to the north [14]. Terrane accretions and terrane dispersions happened within the late Mesozoic-Cenozoic in the southeastern part of Sundaland and formed Java Island is marked with the grey zone in Figure 5. The Java Island is composed of several parts, which are the southeastern corner of the Eurasia Continental Plate, terrane accretions, and micro-plate originating from northern Gondwana-Land. The micro-plate of Gondwana-Land are rifted, drifted, and amalgamated in the late Mesozoic-Cenozoic. There was a collision between Sundaland margins with the fragment of Gondwana Continental in the middle of Cretaceous, where the suture locates at the Meratus Ridge Region [21, 22]. Several micro-plates (terranes) merged into one plate during the docking period in the making of the Java Island as the extensional of the southeastern part of the Sundaland, which is marked as the accreted crust in Figure 5 [20, 23, 24]. During the period, the Indo-Australia Plate movement rate decreasing when the Makasar Strait commenced to the rifting stage. The situation makes a huge structural and tectonics trend changing in Java Island from the Paleogene structures in the northeast-southwest direction transform into Neogene structures in the west-east direction [25].

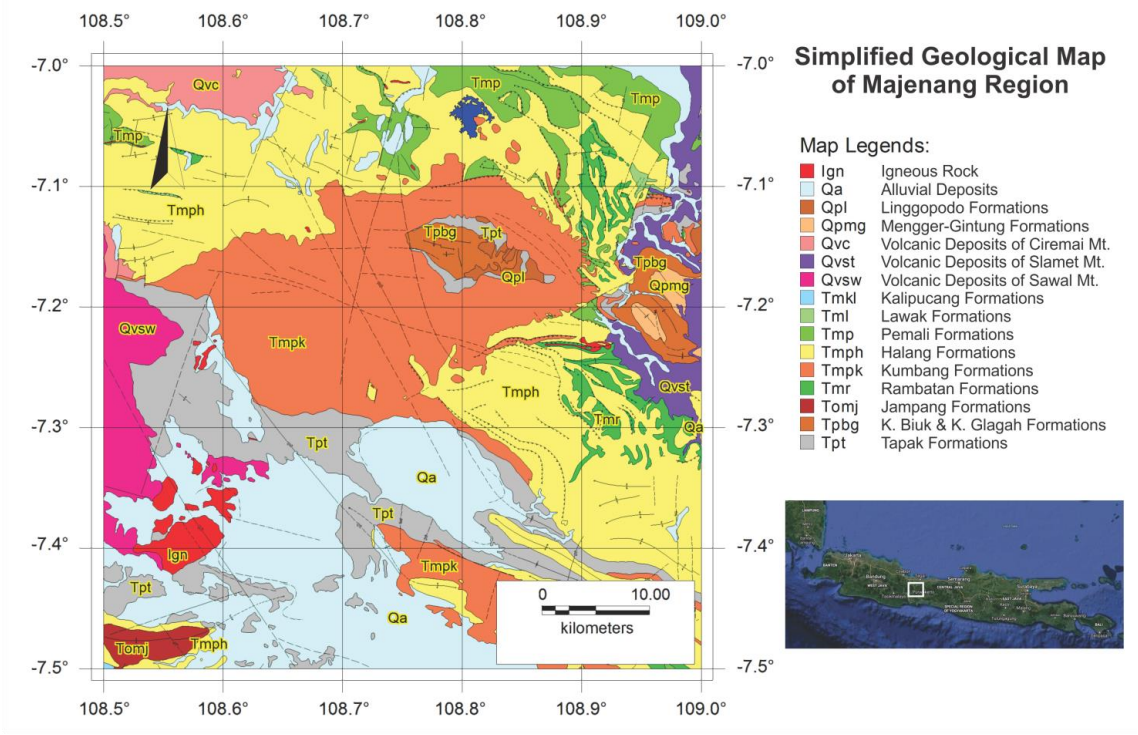

Figure 6. Simplified Geological Map of the Majenang Region.

The Eocene-Oligocene Karangsambung Formation is the oldest-rock located in the Purwokerto Quadrangle as the eastern part of the study area. The late Oligocene-early Miocene Gabon Formation spread out in the Pangandaran Quadrangle as the southern part of the study area. The Gabon Formation composes of andesitic to basaltic volcanic materials, including its tuff members. Andesitic rocks of early Miocene-middle Miocene intrude the Gabon Formation. The Gabon Formation is unconformable underlain by the middle Miocene Pamutuan Formation, which composes of marine sediments and volcanic debris. The Pamutuan Formation spreads out in the Pangandaran Quadrangle as the southern part of the study area. Kalipucang Formation consists mainly of reef limestone, which spreads out in the northern part of the Gabon Formation. Pemali Formation composed of turbidite sediments of the middle Miocene is dominant spreads out at the northeastern and southeastern part of the study area. There is an uncertain relationship between the middle Miocene Pemali Formation and other middle Miocene Formations (such as Pamutuan, Kalipucang, and Penosogan Formation). All of the middle Miocene Formations are interfingering relation with Halang Formation. The middle Miocene-early Pliocene Halang Formation is the youngest turbidite sediment in the study area. The Halang Formation conformably is underlain by the Tapak Formation, which consists of clastic-sediments. A simplified geological map of the study area is shown in Figure 6. The recent known active volcano also presence in the eastern part of the study area, which is called Slamet Volcano. The Older Slamet Volcano recognizes located at the southwestern part of the recent active Slamet Volcano [26].

Spectral analysis method was used to calculate the regional-residual data separation of the Bouguer gravity anomaly. The Bouguer gravity anomaly and the residual gravity dataset are shown in Figure 7a and Figure 7b respectively. According to the residual gravity interpretation, there is a strike-slip fault detected and interpreted as the Pamanukan-Cilacap dextral strike-slip fault as part of the Pamanukan-Cilacap Fault Zone (PCFZ), which consists of Citanduy Fault, Pamanukan-Cilacap Fault, and Ajibarang / Bumiayu Fault [27]. A circular pattern delineated and then interpreted as the part of ring-fault in the Majenang area. The high residual gravity anomaly located within the inferred caldera interpreted as the lava domes or intrusion bodies, which are consists of the Sangkur Mount at the southwestern part of the study area and the Kumbang Mount relatively at the center of the study area. The proposed eruption center in the study area is marked with the red star symbol on the map. A superimposed visualization of the residual gravity anomaly with the geological map of the study area is shown in Figure 8a. The eruption center is predicted based on the low residual gravity dataset and superimposed with the soft sediment of the alluvium (Q_a) on the geological map of the study area as shown in Figure 8a.

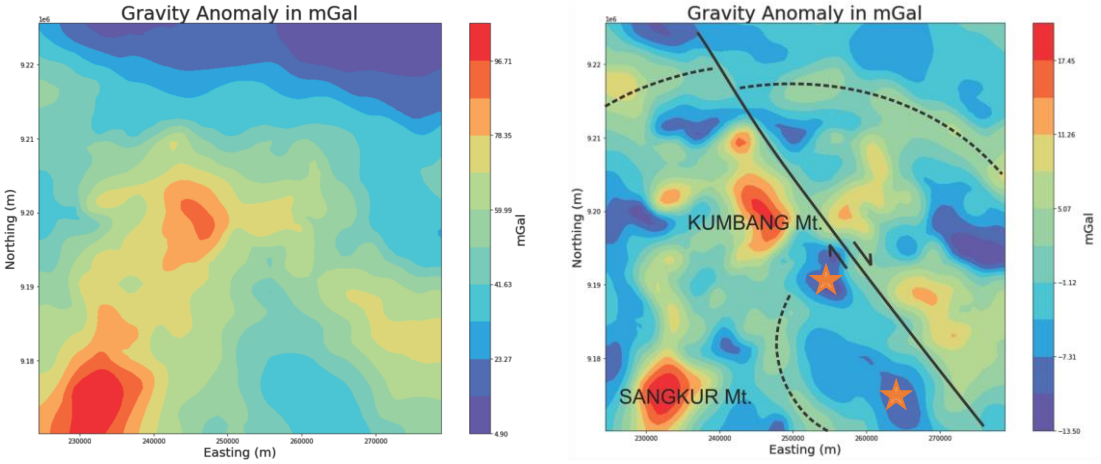

Figure 7. Bouguer gravity anomaly (left) and residual gravity anomaly (right) map of the study area shown respectively. The Pamanukan – Cilacap Fault Zone (PCFZ) marked on the map as the Pamanukan-Cilacap right-lateral strike-slip fault.

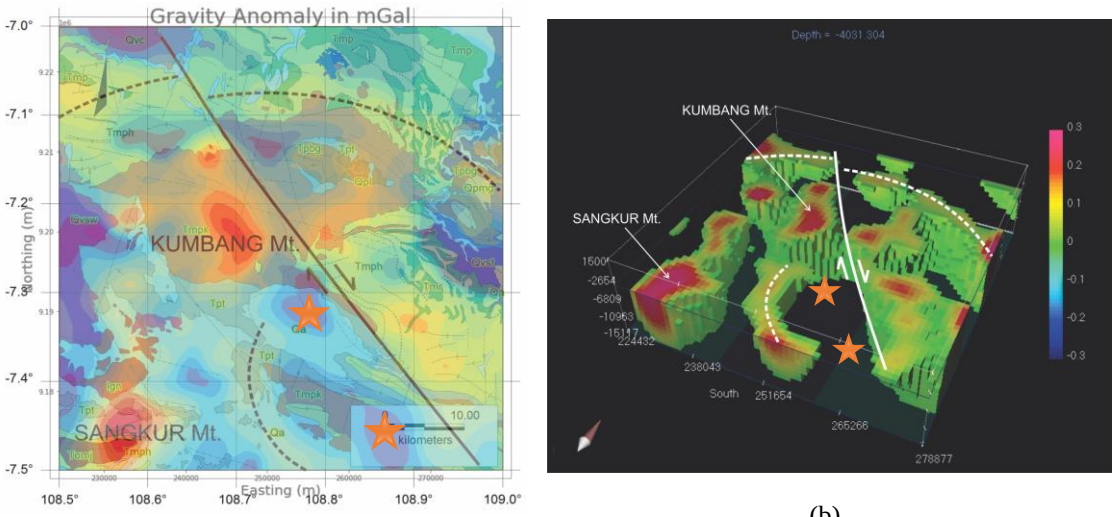

(a) (b)

Figure 8. Residual gravity anomaly map superimposed with the geological map of the study area (a). The causative body model visualized based on the gravity inversion located at the 4031 m depth below the surface in the Majenang region, Central Java, Indonesia (b).

The inversion result at the depth of 4031 m beneath the surface is visualized in Figure 8b with the positive density contrast value. The existing density contrast offset is seen as the dextral strike-slip fault, which is interpreted further as the part of the deep-seated Pamanukan – Cilacap Fault Zone (PCFZ). The circular pattern, which is interpreted as the part of ring-fault / caldera rim clearly imaged in the density contrast model. The predicted eruption center is shown as the void / empty space and marked with the red star symbol in Figure 8b due to allegedly contain of soft volcanic sediments, which is represented by the negative or low density contrast in the inversion result. The relatively rounded high-density contrast bodies interpreted as the lava domes or intrusion bodies of Sangkur Mt. and Kumbang Mt.

A topographic visualization superimposed with the residual gravity anomaly exposed the circular anomaly location is following the outer part of the inferred ring-fault (Figure 9). There are high-density material buried circularly following the outer part of the ring-fault terrain and interpreted as the buried lava. Other high residual gravity anomalies are located at the inner side of the ring-fault (within the inferred caldera) interpreted as lava dome or intrusion body. Further geophysical research is needed to distinguish whether this type of anomalies are lava domes or intrusion bodies. The ancient eruption points are predicted at around Majenang city as shown with the red stars symbol in Figure 9. A comparison between the observed gravity dataset and the calculated gravity dataset is made to examine qualitatively of the inversion

result as shown in Figure 10. According to the Figure 10, the gravity calculated dataset is close enough to the gravity observed dataset. We can conclude that the inversion result is acceptable for further interpretation.

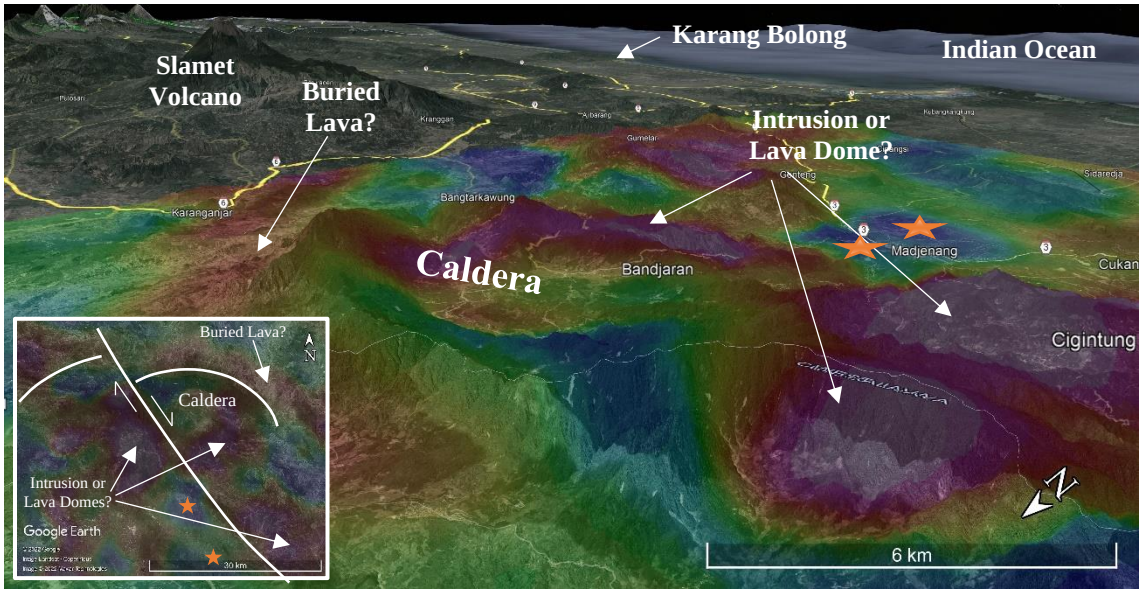

Figure 9. Superimposed visualization both the residual gravity anomaly and the Digital Elevation Model (DEM) with elevation exaggeration parameter set to two. A circular anomaly interpreted as lava surround the ancient volcanic caldera while the high-density anomalies interpreted as the lava domes or intrusion bodies within the caldera.

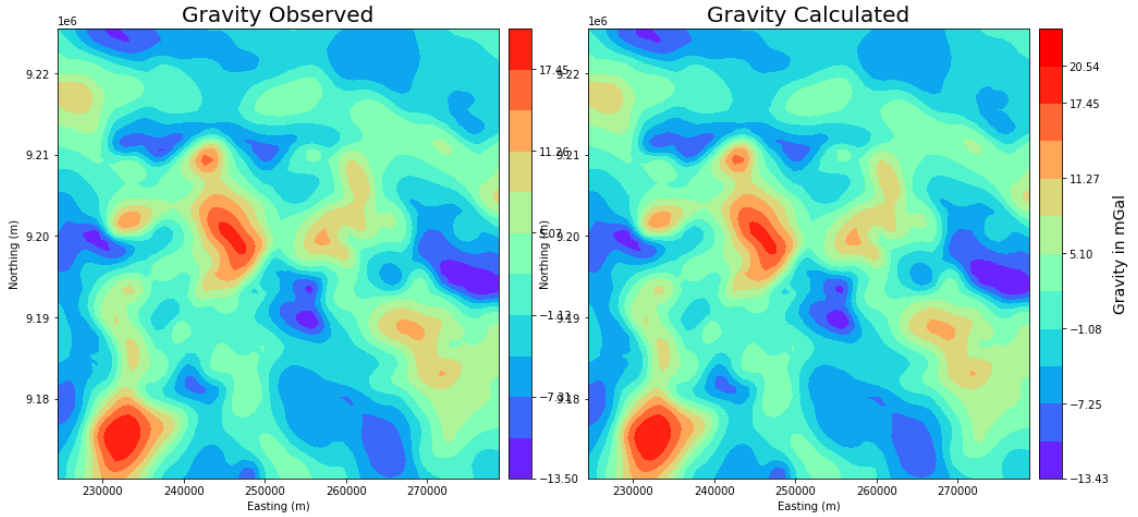

Figure 10. A Comparison of the Gravity Observed dataset and the Gravity Calculated dataset from the inversion modeling result.

IV. CONCLUSION

A ring-fault (caldera-rims) has been identified based on the gravity 3-D inverse modeling in the Majenang region, Central Java, Indonesia. The Pamanukan-Cilacap Dextral Strike-Slip Fault was imaged based on the residual gravity dataset and the inverse modeling result at the depth of 4031 m below the surface. The strike-slip fault delineated in the northwest-southeast direction suggested as a part of the Pamanukan Cilacap Fault Zone (PCFZ). The high-density anomaly distribution found following the circular terrain of topography is interpreted as buried lava in the study area. Other high-density anomalies dominantly located at the inner part of the inferred caldera (inner side of the ring-fault). Those high-density

anomalies are interpreted as the lava domes or intrusion bodies, which are superimposed with Sangkur Mt. and Kumbang Mt. Further geophysical study is needed to provide a better characterization of the anomalies and to justified whether the anomalies are lava dome or intrusion bodies. We proposed that the Pamanukan-Cilacap Fault Zone (PCFZ) manifests as the weak zone in the area, where the magmatism passes through and rises a volcano, which now remain as Majenang Caldera. Hence, the study area is interpreted as the Ancient Volcanic Caldera of Majenang where the eruption point predicted at around Majenang city.

ACKNOWLEDGEMENTS

The authors are most grateful to Director for the Center of Geological Survey, Geological Agency, Ministry of Energy and Mineral Resources (MEMR) of the Republic of Indonesia for all the support and research opportunity. We also sincerely thank the reviewers for their valuable suggestions for the improvement of this paper.

REFERENCES

[1] B. J. Last and K. Kubik, "Compact gravity inversion", *Geophysics*, vol. 48, no. 6, pp. 713–721, 1983. doi: 10.1190/1.1441501.

[2] A. G. Camacho, F. G. Montesinos, and R. Vieira, "Gravity inversion by means of growing bodies", *Geophysics*, vol. 65, no. 1, pp. 95–101, 2000. doi: 10.1190/1.1444729.

[3] L. Uieda, and V. C. F. Barbosa, "Robust 3D gravity gradient inversion by planting anomalous densities", *Geophysics*, vol. 77, no. 4, pp. G55–G66, 2012. Doi: 10.1190/geo2011-0388.1.

[4] M. H. P. Bott, "The use of Rapid Digital Computing Methods for Direct Gravity Interpretation of Sedimentary Basins", *Geophysical Journal of the Royal Astronomical Society*, vol. 3, no. 1, pp. 63–67, 1960. Doi: 10.1111/j.1365-246X.1960.tb00065.x.

[5] L. Cordell, and R. G. Henderson, "Iterative Three-Dimensional Solution of Gravity Anomaly Data Using A Digital Computer", *Geophysics*, vol. 33, no. 4, pp. 596–601, 1968.

[6] R. C. Jachens and B. C. Moring, "Maps of the thickness of cenozoic deposits and the isostatic gravity over basement for nevada", *US Geological Survey*, Report 90, 1990.

[7] R. W. Saltus, "Upper-crustal structure beneath the Columbia River Basalt Group, Washington: gravity interpretation controlled by borehole and seismic studies", *Geological Society of America Bulletin*, vol. 105, no. 9, pp. 1247–1259, 1993. Doi: 10.1130/0016-7606(1993)105<1247:UCSBTC>2.3.CO;2.

[8] X, Zhou "Gravity inversion of 2D bedrock topography for heterogeneous sedimentary basins based on line integral and maximum difference reduction methods", *Geophysical Prospecting*, vol. 61, no. 1, pp. 220–234, 2013. Doi: 10.1111/j.1365-2478.2011.01046.x.

[9] A. Handyarso and H. Grandis "Three-dimensional gravity inverse modeling for basement depth estimation integrating maximum difference reduction (MDR), trend surface analysis (TSA) and total variation regularization", *Journal of Engineering and Technological Sciences*, vol. 49, no. 3, pp. 358–372, 2017. doi: 10.5614/j.eng.technol.sci.2017.49.3.5.

[10] J. B. C. Silva, D. F. Santos, and K. P. Gomes, "Fast gravity inversion of basement relief", Geophysics, vol. 79, no. 5, pp. G79–G91, 2014. Doi: 10.1190/GEO2014-0024.1.

[11] M. S. Zhdanov, *Geophysical inverse theory and regularization problems*. Edition. City: Publisher. 2002: pages.

[12] W. A. Lima, *et al*. "Total variation regularization for depth-to-basement estimate: Part 2 — Physicogeologic meaning and comparisons with previous inversion methods", *Geophysics*, vol. 76, no. 1, pp. I13–I20, 2011. doi: 10.1190/1.3524547.

[13] S. Bronto, "Fasies gunung api dan aplikasinya", *Indonesian Journal on Geoscience*, vol. 1, no. 2, pp. 59–71, 2006. doi: 10.17014/IJOG.1.2.59-71.

[14] R. Soeria-Atmadja, et al. "Tertiary magmatic belts in Java", Journal of Southeast Asian Earth Sciences, vol. 9, no. 1–2, pp. 13–27, 1994. Doi: 10.1016/0743-9547(94)90062-0.

[15] S. Bachri, *Pengaruh kegiatan tektonik & vulkanisme terhadap sedimentasi endapan paleogen-neogen di cekungan Serayu, Jawa*. First edition. Bandung: LIPI Press. 2017: 141.

[16] R. J. Blakely, *Potential theory in gravity and magnetic applications*. Edition. City: Cambridge University Press. 1995. doi: 10.1017/CBO9780511549816.
[17] H. Grandis, *Pengantar pemodelan inversi geofisika*. Edition. City: Publisher. 2009: pages.
[18] J. A. Katili, "Geochronology of west indonesia and its implication on plate tectonics", *Techtonophysics*, vol. 19, pp. 195–212, 1973.
[19] J. A. Katili, "Volcanism and plate tectonics in the Indonesian island arcs", Tectonophysics, vol. 6, no. 3–4, pp. 165–188, 1975. Doi: 10.1016/0040-1951(75)90088-8.
[20] A. H. Satyana, "Accretion and dispersion of southeast sundaland: the growing and slivering of a continent", Proceedings of Joint Convention Jakarta, Indonesia, 2003.
[21] K. Wakita, *et al*. "Tectonic implications of new age data for the Meratus Complex of south Kalimantan, Indonesia", *Island Arc*, vol. 7, no. 1–2, pp. 202–222, 1998. doi: 10.1046/j.1440-1738.1998.00163.x.
[22] R. Hall, B. Clements, H. R. and Smyth, "Sundaland: basement character, structure and plate tectonic development", *Proceedings Indonesian Petroleum Association 33rd Annual Convention*, (July), pp. 1–27, 2009. doi: 10.29118/ipa.2374.09.g.134.
[23] H. Satyana, "New consideration on the cretaceous subduction zone of ciletuh-luk ulo-bayat-meratus: implications for southeast sundaland petroleum geology", *Proceedings Indonesian Petroleum Association Annual Convention*, (May), 2018. doi: 10.29118/ipa.0.14.g.129.
[24] I. Metcalfe, "Tectonic framework and Phanerozoic evolution of Sundaland", Gondwana Research. *International Association for Gondwana Research*, vol. 19, no. 1, pp. 3–21, 2011. doi: 10.1016/j.gr.2010.02.016.
[25] S. Bachri, "Pengaruh tektonik regional terhadap pola struktur dan tektonik Pulau Jawa", *Geologi dan Sumberdaya Mineral*, vol. 15, no. 4, pp. 215–221, 2014.
[26] I. S. Sutawidjaja, "Cinder cones of Mount Slamet, Central Java, Indonesia", Indonesian Journal on *Geoscience*, 4(1), pp. 57–75, 2009. Available at: http://ijog.bgl.esdm.go.id.
[27] C. Armandita, et al. "Trace of the translated subduction in central Java and its role on the Paleogene basins and petroleum system development", *Proceedings JCM makassar 2011 The 36th HAGI and 40th IAGI Annual Convention and Exhibition Makassar*, 26 – 29 September 2011, (September), pp. 26–29, 2011.